Chapter 2

High-Power Diode-Pumped Short Pulse Lasers Based on Yb:KGW Crystals for Industrial Applications

Guang-Hoon Kim, Juhee Yang, Byunghak Lee, Bosu Jeong, Sergey Chizhov, Elena Sall, Vladimir Yashin and Uk Kang

Additional information is available at the end of the chapter

http://dx.doi.org/10.5772/64571

Abstract

A diode-pumped, ultrafast Yb:KYW laser system utilizing chirped-pulse amplification (CPA) in a dual-slab regenerative amplifier (RA) with spectral shaping of seeding pulse from a master oscillator (MO) has been developed. A train of compressed pulses with pulse length of 181 fs, repetition rate up to 500 kHz, and average power exceeding 15 W after compression and pulse picker was achieved.

Keywords: lasers, diode-pumped, laser amplifiers, solid-state lasers, ytterbium lasers, ultrafast lasers, mode-locked lasers, ultrafast lasers

1. Introduction

Energetic (dozens of μJ) optical pulses with femtosecond (fs) pulse lengths and hence ultrahigh focused intensities in the range of 10^{12}–10^{16} Wcm^{-2} are capable of ablating a wide range of materials including metals, semiconductors, ceramics, polymers, biological tissue, and dielectrics [1–3]. Femtosecond laser ablation has been demonstrated to be a powerful tool for various technologies [2]. Due to rapid energy delivery, the laser-plasma interaction is avoided and heat-affected zones in the irradiated targets are strongly localized with minimal residual damage. This allows generation of well-defined microstructures with high quality and reproducibility [1–3].

Femtosecond laser sources based on Yb-doped laser materials became promising tool for various technological and industrial applications including femtosecond lasers. Among Yb-media ytterbium tungstates (Yb:KYW/Yb:KGW), crystals Yb:KY$(WO_4)_2$ (Yb:KYW) or Yb:KGd$(WO_4)_2$ (Yb:KGW) exhibits an attractive set of parameters that makes it as one of the best choices for high-power fs lasers operating around 1 μm [4]. Bandwidth of Yb:KGW/Yb:KYW is sufficient for amplification of sub-200 fs pulses, but typical pulse length on the output of Yb:KYW amplifier system is limited on the level 300–400 fs [5, 6] primarily due to gain narrowing [7, 8]. A promising method to reduce the effect of gain narrowing and to increase the effective gain bandwidth is to combine laser media with separated gain maxima and to overlap broadband gain. Using Yb:KYW crystals with different orientation of crystallographic axes, e.g. N_g- and N_p-cut orientation, this approach has been realized in [9]. Another way for increasing gain bandwidth is using special spectral filters introducing controlled losses at maximum gain spectrum [7].

In this review chapter we present combination of those approaches to a double-slab regenerative amplifier (RA). Each slab is pumped separately, which enables additional possibility to control gain. Furthermore as a seed source, we used high-power master oscillator (MO) based on N_p-cut Yb:KYW crystal with output pulse length ~100 fs and central wavelength agreed well with spectral gain profile of regenerative amplifier. A highly efficient stretcher and compressor based on single transmitted diffraction grating are used for stretching and recompressing initial pulses after master oscillator.

2. Design of high-average power Yb:KGW laser system

The laser was realized as a chirped-pulse amplification (CPA) system [10]. The system shown in **Figure 1** consists of a femtosecond master oscillator (MO) based on Yb:KGW crystal, a

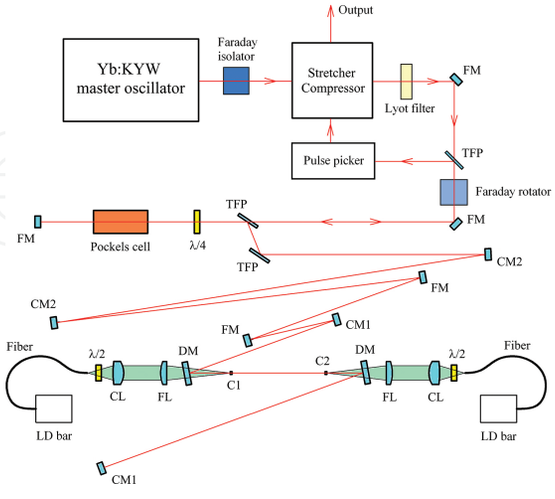

Figure 1. Schematic layout of the femtosecond laser system [15]. FM is a high reflective flat mirror; CM1 is a curved mirror with ROC = 400 mm; CM2 is a curved mirror with ROC = 600 mm; DM is a flat dichroic mirror; FL is a focusing lens; CL is a collimating lens; C1 and C2 are Yb:KYW crystals; TFP is a thin film polarizer; λ/4 is a quarter wave plate; λ/2 is a half wave plate.

http://dx.doi.org/10.5772/64571

common module of stretcher and compressor based on single diffraction grating, a spectral shaper based on Lyot filter, and a dual-slab regenerative amplifier (RA) with combined gain spectra. The system also includes two Faraday isolators: one for isolation of MO against leaking amplified pulses and the other for extraction of laser pulses from the system after RA. To increase the contrast ratio of output pulses according to pre-pulses and post-pulses, we used a pulse picker based on a second Pockels cell and a few thin film polarizers (TFP) with high quality.

2.1. Mode-locked Yb:KYW oscillator

A schematic design of the Yb:KYW oscillator is shown in **Figure 2**. As a gain material, we used a 3×3×3 mm at 5% Yb^{3+}-doped KGW crystal with antireflection-coated ends both for the pump radiation and for the lasing radiation. The crystal was used in an N_g-cut (N_p-cut) geometry, such that the laser polarization was aligned along the N_p axis (N_m axis), respectively. The pump beam from the 100 μm core diameter fiber output was collimated by an achromatic doublet (CL) with focal length F = 60 mm. Then the beam was focused into the laser crystal (LC) by another achromatic doublet (FL) with focal length F = 60 mm through special dichroic coated mirror (DM1) with transmittance of 95%. By using three chirped mirrors with group-velocity dispersion −1350 fs^2 per single pass, the dispersion in the laser cavity was compensated. The details of the optical layout of the laser are described in Ref. [11]. The concave mirror in the second arm of the cavity was replaced by dichroic coated mirror (DM2) with radius of curvature R = 100 mm and a dumper (d) is mounted additionally. Therefore, the pump beam can transmit through the dichroic mirror DM2 and laser operation can be more stabilized without heating optical mounts of mirror M3.

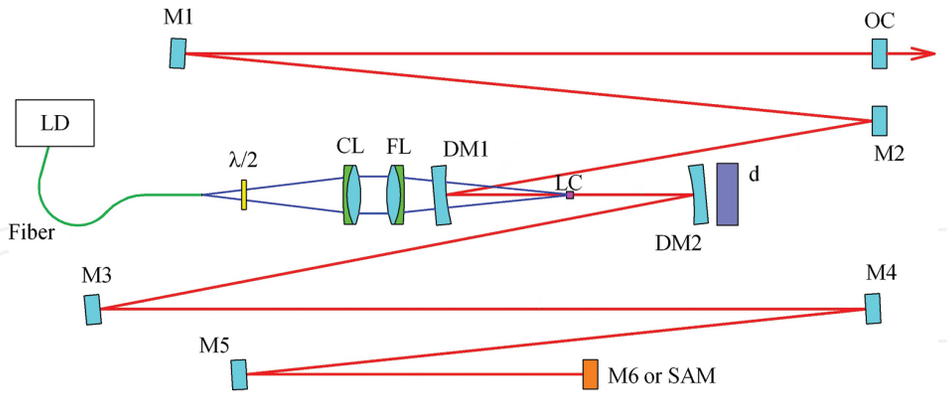

Figure 2. Schematic diagram of the Yb:KYW laser pumped by laser diode (LD) [25]. λ/2 – half wave plate; CL – collimating lens; FL – focusing lens; LC – Yb:KYW laser crystal; DM1, DM2 – spherical dichroic mirror; M1–M6 – cavity mirrors; OC – output coupler; SAM – semiconductor saturable-absorber mirror; d – dumper for blocking and cooling.

As is well known, the transverse size of the pump zone should match with the size of the cavity mode to achieve maximum output power. **Figure 3(a)** shows the schematic drawing to assist in understanding the mode matching between the cavity mode and pump. The pump beam is focused onto the laser crystal as shown in **Figure 3(a)** with black lines and the cavity mode is

depicted as pink color. The position of laser crystal can be defined by the displacement x from the center of the caustic of the beam in the cavity. When the crystal is located in the caustic center of the cavity mode (x = 0 mm), the pump size is larger than the size of cavity mode. Optimal matching of cavity mode and pumped zone in the active media is important for an efficient laser operation. But it is not easy to match the pump size to cavity mode by changing the specification of pump module, because the conventional optics such as fiber and lens are limited in core size and focal length. Instead, mode matching can be easily achieved by displacing the crystal longitudinally along the optical axis. The comparison of the beam profile of pump and cavity mode for both cases of displacement x = 0 mm and 3.5 mm clearly shows this phenomenon as shown in **Figure 3(c)** and **(d)**. The pump profile was obtained by using ZEMAX optical system design software. The cavity mode is assumed to have Gaussian profile and the relevant factors are obtained from LASCAD simulation [12].

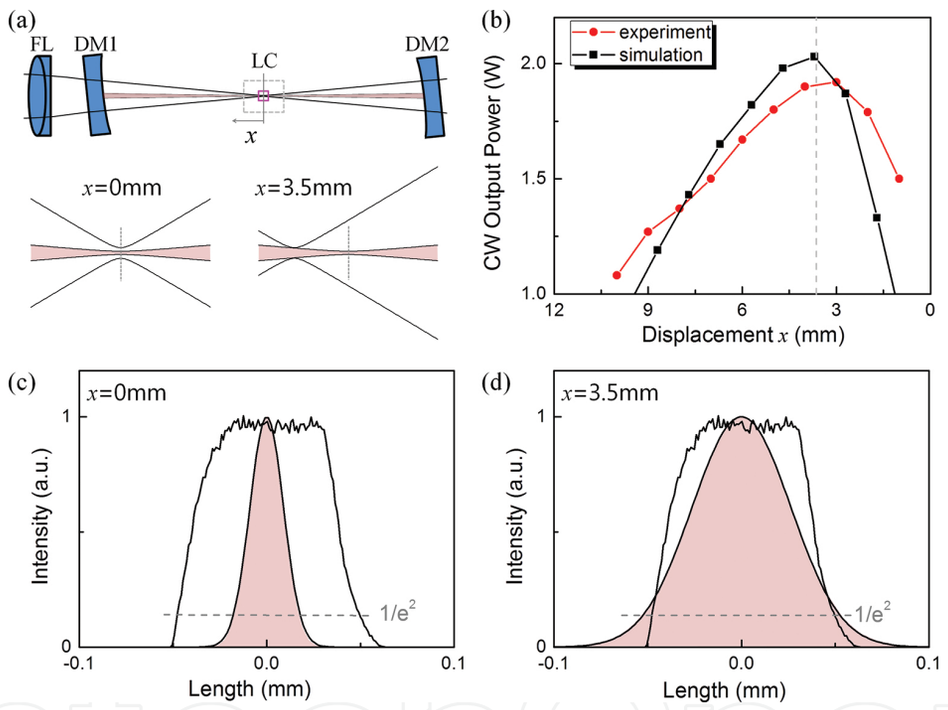

Figure 3. (a) Schematic diagram for the definition of displacement x from the center of the caustic of the beam in the cavity and for the understanding of mode matching. (b) CW output power versus position of laser crystal in the cavity for N_g-cut crystal with OC = 4% of experiment (red) and simulation (black). Comparison of beam profile between pump and cavity mode is shown in the condition of (c) x = 0 mm and (d) x = 3.5 mm [26].

To optimize the position of the crystal, we calculated the CW output power of the resonator as a function of the displacement x as depicted in **Figure 3(b)** with black dots and line by using the LASCAD software. In LASCAD simulation we approximate the top-hat pump spot in focal plane of FL as super-Gaussian distribution in xy plane with diameter 100 μm ($1/e^2$ level). Calculated cavity mode diameter between two curved mirrors DM1 and DM2 significantly changes from diameter 36 μm in a waist to 1.5 mm on the mirror. **Figure 3(b)** shows that the optimal position of the crystal is ~3.5 mm apart from the center of the beam caustic. In order to check the mode matching simulation, we performed the experiment with N_g-cut crystal

http://dx.doi.org/10.5772/64571

oscillator, which was developed previously and in a same condition with simulation [11]. As shown in **Figure 3(b)** with red dots and line, the CW output power is highly dependent on the position of laser crystal and the experimental result coincides well with simulation result. As a note, multimode operation occurred in experiment when the size of the pump beam is larger than TEM_{00} cavity mode and it causes higher CW output power in the displacement region below 3.5 mm.

Not only the position of crystal in the cavity but also the amplification axis of crystal affects the laser operation greatly, because the absorption and emission cross sections of the crystal are quite different according to the orientation of the crystal. In previous work [11], we chose a lasing with $E//N_p$ for antireflection-coated slab crystal because of its broader emission spectrum [6]. We obtained the generator's average power exceeding 1 W at the central wavelength of 1043 nm with a pulse about 90 fs wide. But, according to the literature [13], laser can operate in the shorter wavelength range than 1043 nm by using the different amplification axis of the crystal such as $E//N_m$. For providing effective amplification as a seeding source of CPA femtosecond laser system, the oscillator with shorter wavelength such as 1030 nm is more suitable than the one with 1043 nm [14, 15].

Before going into experiments, we compare the CW output power of the oscillator between N_p- and N_m-polarization with respect to the transmission of output coupler with LASCAD simulation. The corresponding output powers for N_p- and N_m-polarization crystals are shown in **Figure 4(a)** as black and red dots and lines, respectively. From the simulated results, we can conclude that N_m-polarized crystal with 6% output coupler can be used as a candidate for the purpose of seeding source, since only the center wavelength would change with similar output power when we replace the crystal from N_p-polarization (N_g-cut) to N_m-polarization (N_p-cut). And the transmission of 6% of output coupler is chosen due to the output power saturation near 6%.

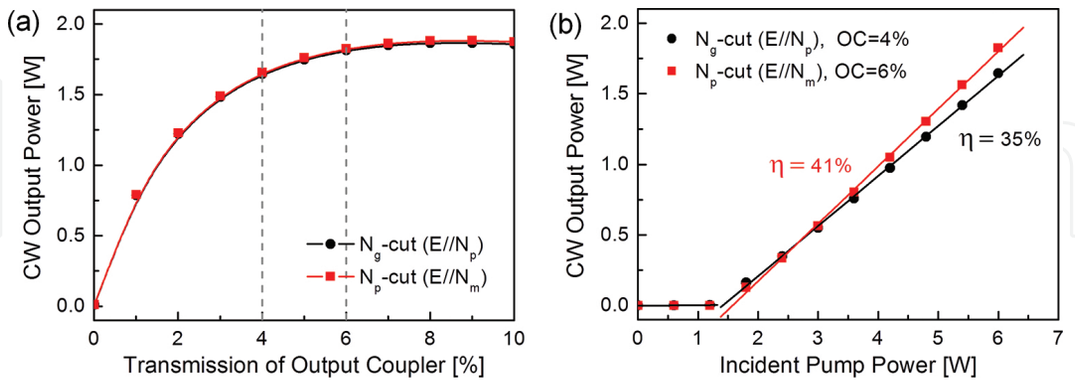

Figure 4. (a) CW output power versus transmission of output coupler for both the N_p- and N_m-polarized crystal. (b) CW output power versus incident pump power for N_p- (OC = 4%) and N_m-polarized crystal (OC = 6%) [26].

Figure 4(b) shows the simulated results according to the replacement from N_p-polarized crystal with 4% output coupler to N_m-polarized crystal with 6% output coupler, in point of the dependence of the average output power on the incident pump power. The slope efficiency

with respect to the incident radiation power is 41% and 35% for each condition. From the simulation results, it is expected to get high output power and high slope efficiency with more suitable center wavelength in the new oscillator.

Based on the simulation results, we conducted the experiment for femtosecond laser based on N_m-polarization Yb:KYW with 6% output mirror and compared the result with the previously reported oscillator based on N_p-polarization Yb:KYW with 4% output mirror in Ref. [11]. An experimental setup of the laser is presented in **Figure 2** as mentioned above. An 8 W high-brightness InGaAs semiconductor injection laser module coupled into optical fiber with a 105 μm core diameter (0.11 NA) and 10 cm length was employed for optical pumping. By using the thermoelectric element (a Peltier cell), the temperature of the laser diode was adjusted for displacing its wavelength to the absorption maximum in the laser crystal. The crystal had a slab design to facilitate efficient heat removal and placed on the optimized position, 3.5 mm apart from the center of the caustic of the beam in the cavity in the longitudinal direction, for size matching of the pump beam and the cavity modes as mentioned. All the laser elements were placed in a compact one-body housing case with 424×214×84-mm size for stable laser operation.

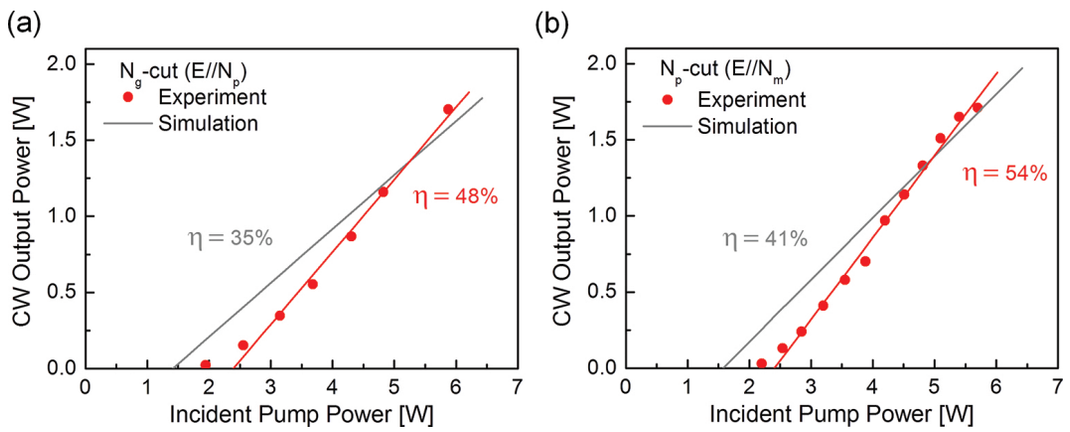

Figure 5. Experimentally observed CW output power versus incident pump power for (a) N_p-polarization (OC = 4%) and (b) N_m-polarization (OC = 6%). Gray lines indicate the calculated values from the LASCAD simulation for comparing with the experimental data [26].

The performance of the laser in the CW regime is shown in **Figure 5** for two cases of (a) the N_p-polarization crystal with 4% output coupler and (b) the N_m-polarization crystal with 6% output coupler. The high slope efficiency of 54% with respect to the incident pump power was achieved with N_m-polarization and the maximum output power exceeded 1.5 W at incident pump power of 6 W. For comparison, simulated CW output powers using LASCAD are also shown in **Figure 5** as grey lines. Computational simulations coincide well with experimental results in general, especially on high incident pump power. The discrepancy in CW output power between experiment and simulation for the low incident pump power can be explained by the characteristics of laser diodes [16]. The center wavelength of diode lasers typically depends on the injection current, operating temperature, and composition. In our case, the operating temperature of the laser diode was adjusted to 36.5°C in high injection current,

http://dx.doi.org/10.5772/64571

corresponding to around 5 W incident pump power in **Figure 5(a)** and **(b)**, for the maximum absorption in the laser crystal. As the injected electric current of laser diode decreases, the pump light shifts toward shorter wavelengths, which results in the decreasing of pump absorption efficiency and low output power of oscillator.

We shall note that for quasi three-level laser media it is difficult to estimate the absorbed pump power experimentally because of the effect of absorption saturation appearing in such media. Therefore we considered the power of launching pump radiation for an estimation of laser efficiency instead of the absorbed power.

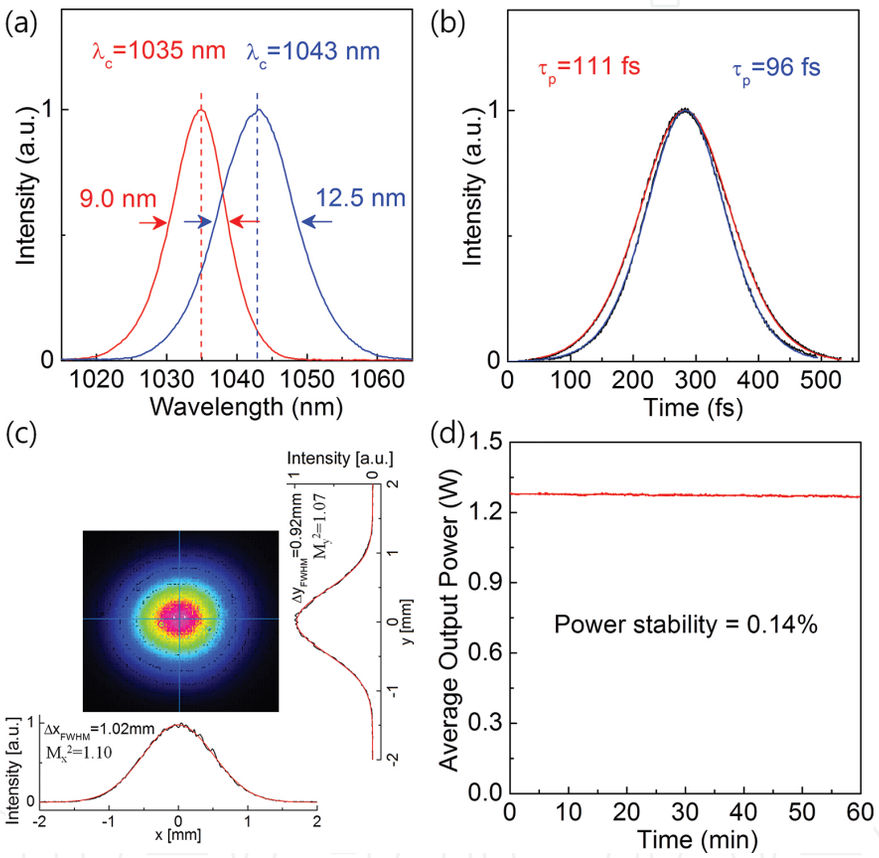

Figure 6. (a) Optical spectra and (b) autocorrelation traces of the 96 fs pulses with center wavelength 1043 nm for N_p-polarization (blue lines) and the 111 fs pulses with center wavelength 1035 nm for N_m-polarization (red lines). (c) Typical spatial pattern of the beam and the corresponding intensity profiles. (d) Measured average output power and its temporal stability [26].

The passively mode-locked regime was realized by replacing a cavity mirror M6 to semiconductor saturable-absorber mirror (SAM) at one end of the resonator in the focal region of a concave mirror (M5) with a radius of curvature R = 300 mm. In **Figure 6(a)** and **(b)**, the measured emission spectra and autocorrelation traces with the fit assuming a sech^2-pulse shape are shown for the N_p- and N_m-polarization as blue and red line, respectively. For N_p-polarization (N_g-cut), 96 fs pulses were generated with the emission spectra centered at

1043 nm. Using N_m-polarization (N_p-cut) crystal, the center wavelength could be changed to 1035 nm with only somewhat longer pulse durations of 111 fs. The time-bandwidth-product of 0.308 is almost close to the Fourier-transform-limited pulse with an intensity profile described by the $sech^2$ function, and it indicates that dispersion is well compensated and there is no frequency modulation.

Typical spatial pattern of the beam at a distance of 1 m from the output coupler for the new oscillator based on N_m-polarization (N_p-cut) crystal is shown in **Figure 5(c)** with the vertical and horizontal intensity profiles. The cross section is nearly Gaussian with horizontal width 1.02 mm and vertical width 0.92 mm. The M^2 values of the beam are 1.10 in the horizontal plane and 1.07 in the vertical plane, which are fairly close to $M^2 = 1$ for an ideal Gaussian beam.

The thermal lens in the laser crystal did not affect the quality of output beam due to weakness of thermo-optical effects. Our calculations with LASCAD show that the focal lengths of thermal lens are 1273 and 1063 mm for horizontal and vertical directions, respectively, that are much larger than the focal length of focusing mirrors.

Figure 5(d) shows the average output power and its stability of the N_m-polarization oscillator after it was warmed up. We have achieved a maximum average power of 1.27 W at a pulse repetition rate of 87.8 MHz, and it gives a single femtosecond pulse energy greater than 14 nJ. The stability of the output power is to be 0.14% by using the definition such as twice the standard deviation of the measured output power divided by the mean output power.

As a summary, a comparison between the laser performances of the N_p- and N_m-polarization (N_g- and N_p-cut) Yb:KYW materials is given in **Table 1**. Both the relative beam angular stability and relative beam positional stability were measured by using the factors related with angular movement and beam positional movement in accordance with ISO 11670 [17]. The achieved parameters show that the new oscillator with N_m-polarization (N_p-cut) crystal is more stable and powerful with well-defined center wavelength as a seeding source.

	λ_{center} (nm)	$\Delta\lambda$ (nm)	P_{output} (W)	τ_p (fs)	M^2	Power stability (%)	Positional stability (%)	Angular stability (%)
E//N_p,	1043	12.5	0.64	96	1.10 (*x*)	0.30	0.5 (*x*)	0.3 (*x*)
OC = 4%					1.25 (*y*)		3.2 (*y*)	1.9 (*y*)
E//N_m,	1035	9.0	1.27	111	1.10 (*x*)	0.14	0.1 (*x*)	0.2 (*x*)
OC = 6%					1.07 (*y*)		0.15 (*y*)	0.3 (*y*)

Table 1. Comparison between N_p- and N_m-polarization Yb:KYW mode-locked oscillators with 4% and 6% output coupler, respectively.

2.2. Stretcher-compressor

Optical pulse stretcher and compressor are a key subsystem in CPA laser systems [10]. In those systems, the stretcher is used to lengthen optical pulses before the amplification, and the compressor is used to restore original short pulses. In this way, the peak power inside the amplifier cavity can be kept low enough to avoid any damage to the optical element and to

http://dx.doi.org/10.5772/64571

suppress nonlinear distortions on the pulse temporal shape and beam spatial profile due to the self-focusing effect.

Design of stretcher and compressor module in a commercial laser system must provide maximum stretched pulse duration and good output spatial and temporal beam quality in minimum module size. To improve total efficiency and make design of stretcher and compressor more compact, we used in our stretcher-compressor module common transmission diffraction grating and folding mirrors (**Figure 7**).

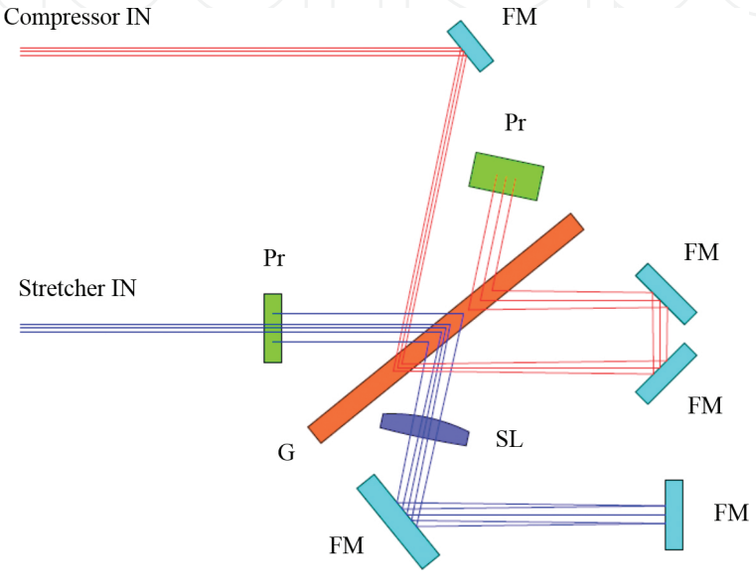

Figure 7. Optical scheme of the stretcher-compressor module based on the transmission diffraction grating (G), spherical lens (SL), right-angle prisms (Pr), and folding mirrors (FM).

In the stretcher and compressor, the beam enters and passes through transmission grating four times. In the stretcher, the beam after first and third passes through diffraction grating is focused and collimated by the spherical lens (SL). To change chirped-pulse duration, we used diffraction grating with two groove densities: N = 1700 mm^{-1} and N = 1500 mm^{-1} and two different spherical lenses with focal length F = 100 mm and F = 200 mm with NA = 0.25 and NA = 0.12, respectively. Using this stretcher-compressor module, we can supply chirped-pulse duration from 50 ps to 300 ps. The compressed pulse duration varies from 230 to 270 fs depending on the optical elements used. Increasing the chirped-pulse duration up to 300 ps using optical elements, the same aperture results in decreasing of spectral pass bandwidth of stretcher up to $\Delta\lambda$ = 14 nm. Spectral clipping introduced by the aperture of optical elements in stretcher affects a recompression pulse duration and its time-bandwidth product.

Increasing the optics aperture is connected with the proportional increase of linear distances in stretcher (spherical aberration introduced by the spherical lens increase with increasing the NA number). Using the diffraction grating with higher groove density to provide more compact design is limited by increasing third-order dispersion.

To check stretcher-compressor module, we used our master oscillator as seed source. We measured initial pulse length and compressed pulse length after the beam passed through the stretcher and compressor. We also measured quality of a beam and total efficiency of the stretcher and compressor. The stretcher-compressor based on 1500 mm^{-1} grating operating with 50 ps chirped-pulse duration provides better degree of recompression and more short output pulse. It is connected with aberration avoiding due to smaller NA number. The measurements made by CCD camera shows that spatial quality of beam did not change after it passed through stretcher and compressor.

Amplification with different pulse durations shows limitation of maximum output pulse energy by Raman scattering excitation and was measured 150 μJ for chirped-pulse duration 50 ps, 300 μJ for 130 ps, and we expected more than 0.5 mJ for 300 ps. Further increase of the pulse energy needs a longer chirped-pulse duration and an increase of the stretcher-compressor module size.

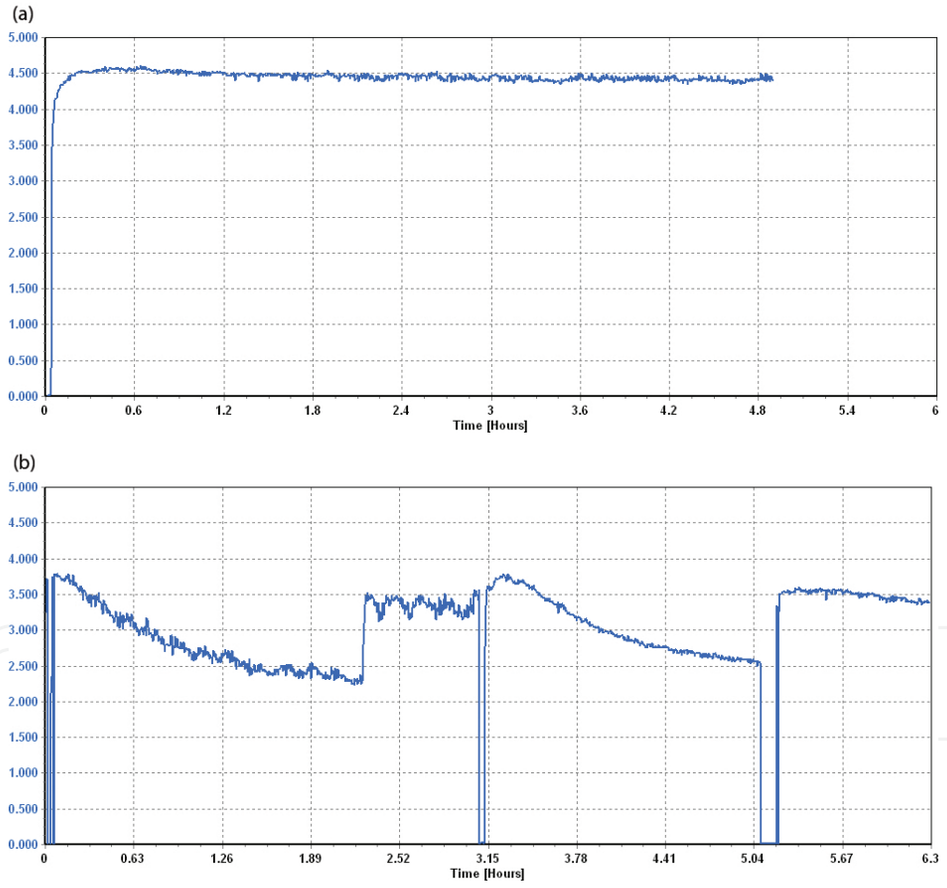

Figure 8. Second harmonic generator output power versus time using thermo stabilized compressor module (a) and nonstabilized one (b).

One of the most important parameters of stretcher-compressor is a temporal stability of compressed pulse duration. Because there is no 100% diffraction grating efficiency, approximately 30% of amplified power is dissipated inside stretcher-compressor module and causes

misalignment of compressor due to thermo expansion of mechanical parts. The requirement for thermomechanical stability of stretcher-compressor elements increases with a decrease in compressed pulse duration. The thermal stabilization of the stretcher-compressor module can significantly improve temporal stability of the compressed pulse. Most dramatically, the effect of temporal detuning of compressor can by observed by the subsequent second harmonic generation. **Figure 8** shows temporal dependence of second harmonic power with water thermo stabilized stretcher-compressor module (a) and without stabilization (b).

In case of no thermo stabilized stretcher-compressor module, fundamental pulse duration increases up to two times with the gradual heating of the module resulting in significant drop of the second harmonic generation efficiency. Thermal stabilization by water cooling the module improves fundamental pulse duration stability and as a result stability of the second harmonic output power.

2.3. Spectral shaping

It is well known that regenerative amplification with high gain leads to the spectral narrowing of amplified pulses [7, 8]. To broaden spectrum in the regenerative amplifier, we tried both extra-cavity and intra-cavity spectral shaping based on the polarization-interference filter (Lyot filter). This technique is well known but it has been used generally for Ti:sapphire lasers [7]. The spectral shaper consists of a birefringent quartz plate placed between two polarizers. To realize optimal spectral shaping, a transmission minimum of the birefringent filter should coincide with maximum gain spectrum and their widths should be close. To fulfill these conditions, a quartz plate with thickness of 8 mm was cut along the optical axis and mounted to the rotation stage to rotate it in two planes for adjusting modulation depth and position of transmission minimum.

2.4. Double-slab laser and amplifier

The maximum average power of solid-state lasers is limited either by the thermal destruction of the active medium or by thermo-optical aberrations [16]. Therefore, one of a few methods of increasing this power in the case of bulk laser media is to increase the active medium length or to use several active elements in the cavity. To increase the average laser power and simultaneously to retain the high spatial quality of the output beam, we used a scheme with two active elements (see also [9, 14, 15]). The optical scheme of a laser amplifier with two active elements made of Yb:KGW crystals with different orientations of optical axes is shown in **Figure 1**. The use of N_p- and N_g-cut crystals, which have different spectral-luminescent characteristics at a corresponding orientation of the polarization vector of generated or amplified beams, makes it possible to widen the gain band and thus generate or amplify more broadband chirped or femtosecond pulses [10]. The crystals were 5 mm long and contained 3% of ytterbium ions, which ensured a good (above 70%) absorption of the pump radiation [18]. Similar to the case of the master oscillator, the pump beam and cavity mode sizes were matched by a longitudinal shift of the active elements. To eliminate possible modulation of the spectrum, the faces of the active elements were antireflection coated and inclined at an angle of ~30′. As pump sources, we used two fiber-coupled laser diode arrays with a maximal output

power of 70 W each. The depolarization of the pump radiation was minimized using a short (30 cm) optical fiber 200 μm in diameter with the numerical aperture NA = 0.22. The pump beams from the fiber output were collimated and focused through dichroic mirrors into the active crystal to a spot with a diameter of about 320 μm, which is close to the diameter of the TEM_{00} cavity mode. This mode was calculated by the well-known ABCD matrix method taking into account the astigmatic thermal lenses induced in the active elements by the pump radiation. Using the LASCAD software, the focal length of these lenses was calculated to be 480–550 mm for the N_p-cut crystal at an incident power of 30 W. These values are in adequate agreement with the literature data [19, 20] and are confirmed by our measurements [18].

We used this laser as a standalone oscillator and as a regenerative amplifier. As an output mirror in this oscillator, we used a thin-film polarizer in combination with a quarter-wave plate, which was rotated to obtain the maximum output power at a given pump power. For electro-optic Q-switching, we used a Pockels cell based on a β-BaB_2O_4 (BBO) crystal and controlled by a special driver. The pulse repetition rate was smoothly changeable from single pulses to 1000 kHz.

The output laser power in the CW regime in the cases of using single active element and two elements simultaneously is shown in **Figure 9** versus the pump power incident on the crystals. The maximum output power was 12.5 and 9 W at a slope efficiency of 47% and 37% for Ng- and Np-cut single crystals, respectively. Note that the output powers for the crystal in which the polarization vector of the laser beam is parallel to the Np axis (E||Np) are higher than for the crystal with E||Nm despite a smaller stimulated emission cross section [9]. This behavior of power can be explained, in our opinion, by different spectral losses in the cavities with crystals emitting at different wavelengths. The maximum output power in the case of two crystals in the cavity was 18.5 W at a pump power of 72 W, which yields the total and slope efficiencies of 25% and 35%, respectively. The laser radiation spectrum was centered at a wavelength of 1035 nm, and its width did not exceed 1 nm.

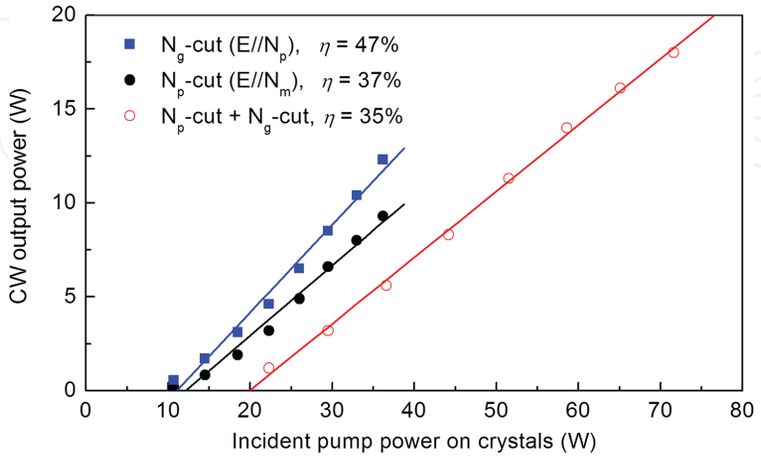

Figure 9. CW output power of laser as a function of incident pump power on crystals in CW mode operation for each single- and dual-slab configuration [15].

http://dx.doi.org/10.5772/64571

Note that the output laser power was maximized in measurements for each pump power by optimal adjustment of the quarter-wave plate. As can be easily shown, this measurement method leads to an underestimation of the slope efficiency. It is this fact that can explain the considerable difference in the slope efficiencies of single- and two-crystal lasers at close total efficiencies (27–30% and 25%, respectively).

The maximum output power obtained in the case of Q-switching reached 16 W at a pulse repetition rate of 100 kHz and 14 W at a repetition rate of 500 kHz (Q-switching time 800 ns). This decrease in the average power with respect to the CW regime can be explained by additional losses introduced by the electro-optic Q-switch. As the Q-switching time decreased to 400 ns, the output power decreased by three times, which obviously occurred because this time was too short for oscillation development. The output pulse duration, determined mainly by a rather long length of the cavity, was 20 ns. The width of the spectrum was 16 nm, which points to a pronouncedly multimode regime. The spectrum had two peaks, at wavelengths of 1035 and 1043 nm, which correspond to the spectral maxima of the gain coefficient for the two used crystals.

We optimized our laser by better alignment of the beam size of pump and laser modes in laser crystals at high pumping levels [21, 22]. This was achieved by moving the mirror CM1 along the optical axis. To suppress thermal losses, the thickness of the laser crystal was also reduced from 2 to 1.2 mm. The optimization results are shown in **Figure 10**. After optimization of the laser, output power increased by 32% from 18.5 to 24.5 W at incident pump power of 110 W.

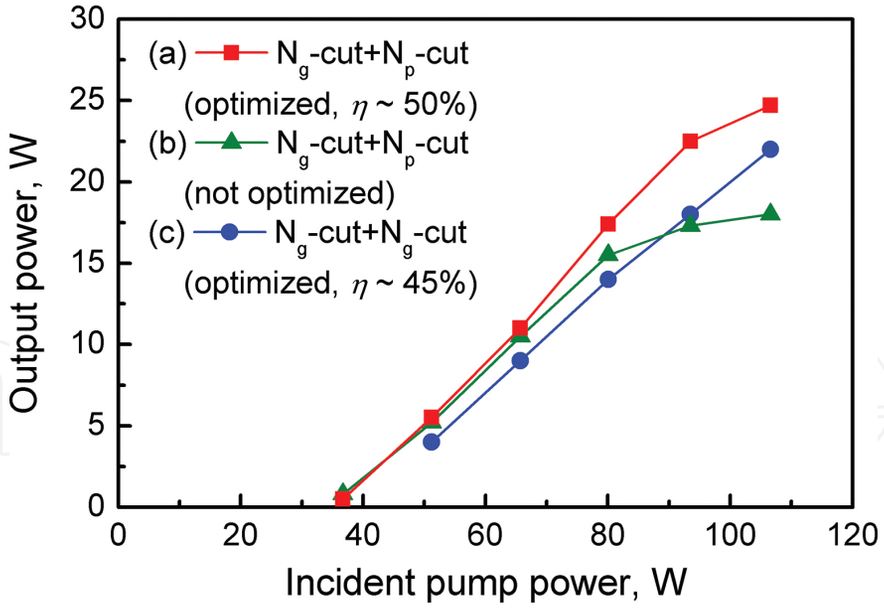

Figure 10. Output power of Q-switched laser versus incident pump power at repetition rate of 200 kHz for different dual-crystal configurations.

Output beam profiles measured using a CCD camera at distance of 1 m from output of compressor was symmetric with beam diameter of 4 mm at e^{-2} intensity level and nearly Gaussian. Increasing of the output power above 15 W resulted in gradual distortion of beam

profile and transformation of beam cross section into the slightly elliptical one as shown in **Figure 5(b)**. However the beam quality parameter M^2 was measured to be below 1.5 even at the laser output power of 22 W as shown in **Figure 11**.

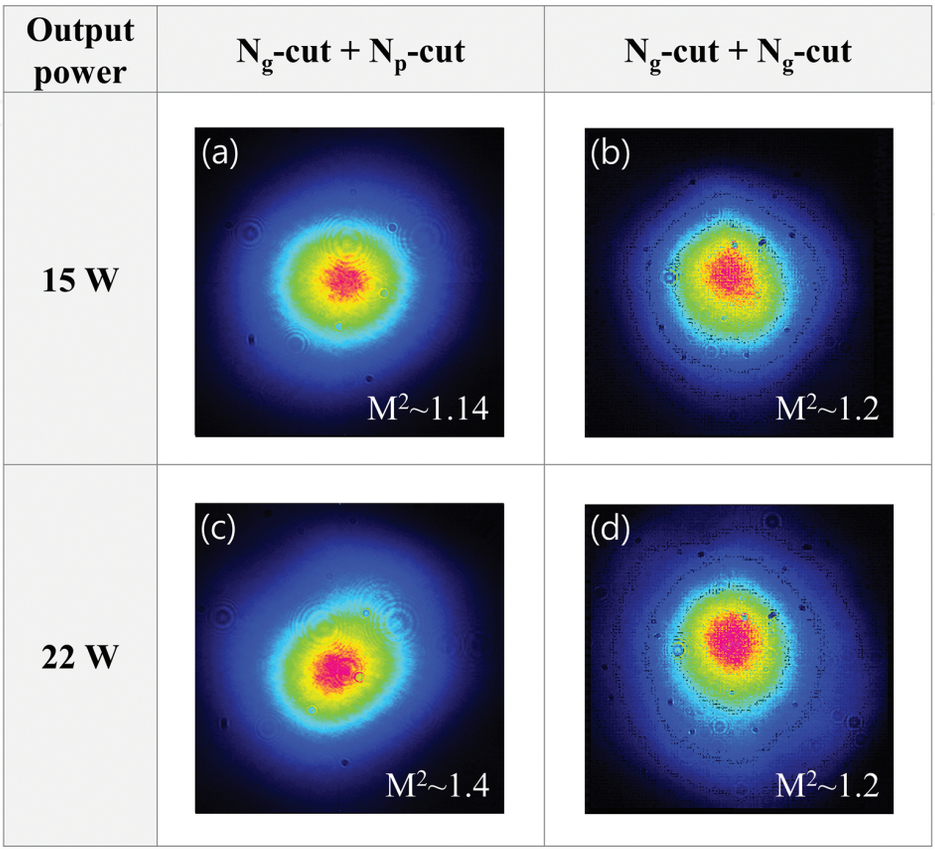

Figure 11. Near-field images and beam qualities M^2 of the laser output for different dual-crystal configurations.

3. Performance of the Yb:KGW femtosecond laser system

When the regenerative amplifier was seeded by stretched pulses, we investigated the output power, spectrum, and pulse shape after compression under different conditions. Our measurements showed that the output power after regenerative amplifier increased up to a value of 21 W when the time gate was increased up to 400 ns and the number of round trips was 24. And then the output power saturated at same value as the time gate increased up to 29 round-trips. It means that the gain is balanced by losses. **Figure 12** shows that the output power is practically linearly dependent on the incident pump power. It means the absence of such parasitic effects restricted gain as amplified spontaneous emission (ASE) and parasitic oscillations. We measured the output power with spectral shaping in addition. There was a power reduction of about 5% when the spectral shaping using a Lyot filter is applied outside the cavity. The compressor and the picker are making a loss, which reduces output power by 25% (15 W).

http://dx.doi.org/10.5772/64571

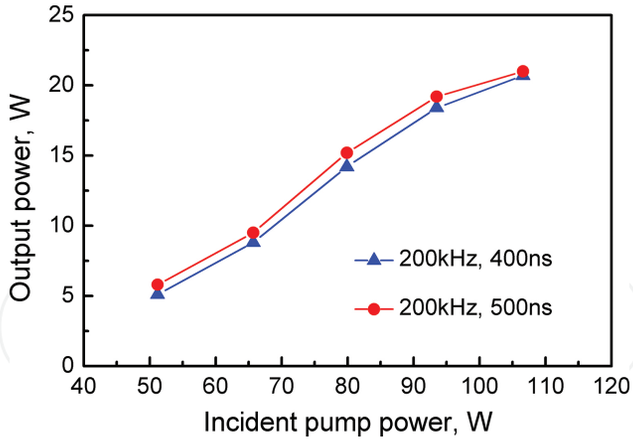

Figure 12. Average output power after RA as a function of incident pump power.

The laser system can operate in the repetition rate range of 50–500 kHz. In this range, the output power is almost not dependent on repetition rate. The single pulse energy was measured to be 300 and 30 μJ at repetition rates of 50 and 500 kHz, correspondently, that is important for microprocessing applications. Maximum pulse energy at 50 kHz was limited by Raman scattering excitation in Yb:KYW crystal that was observed in the experiment [23, 24]. Pulse shape at this repetition rate is distorted phase-modulation of the pulse at the Kerr nonlinearity [24].

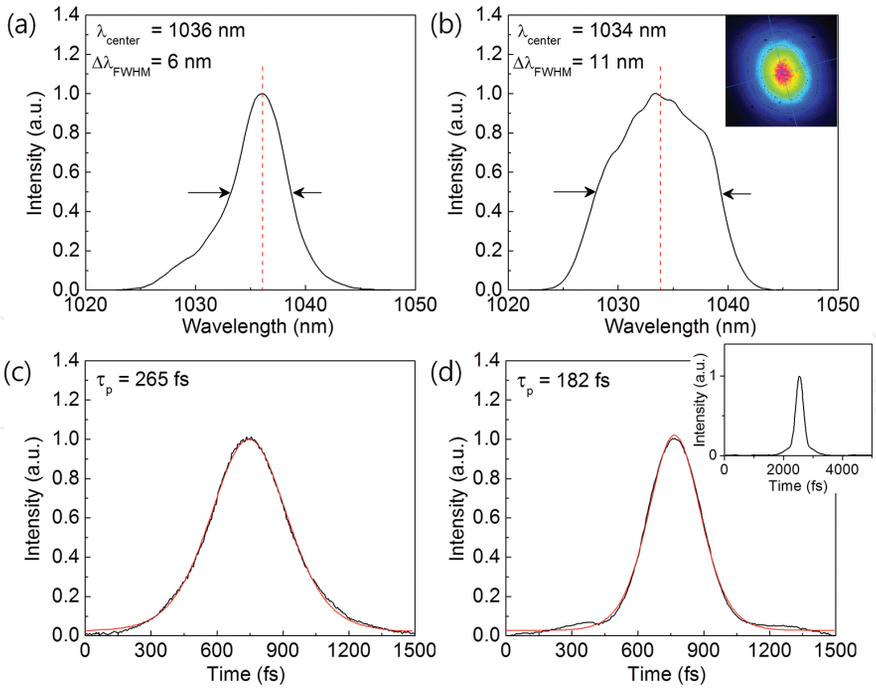

Figure 13. (a, b) Spectra and (c, d) intensity autocorrelation traces (black-experimental data, red-fitting) of output pulses at incident pump power of 67 W and repetition rate of 200 kHz without spectral shaping (a, c) and with spectral shaping (b, d). Insets show the output beam profile (b) and autocorrelation trace in the range of 5 ps (d) [15].

The shape of the output spectrum for equal pump power in both arms of pumping is shown in **Figure 13(a)**. The gain narrowing effect is noticeably well—FWHM spectral width is ~1.5 times narrower compared with the spectrum of master oscillator pulses. Compression provides 265 fs output pulses under this condition as shown in **Figure 13(c)**.

This gain narrowing effect can be suppressed, for example, by making the pump power of Yb:KYW crystals not to be equal [9]. We changed the pump power launched on the N_p-cut and N_g-cut crystals to the ratio of 3:2 [15]. The experimental measurements showed that the spectral width became broader and its shape was modified considerably. In this case, the spectral width was measured to be 11 nm and the pulse length was measured to be 210 fs for assuming sech^2 profile. This method has a drawback that the restriction of pumping power on one crystal results in the restriction of total output power in expense of pulse width. For example the output power dropped 37% in our experimental conditions.

Another way to suppress the spectrum narrowing is to use preliminary spectrum shaping [11] as it was discussed earlier. The example of output spectrum for extra-cavity spectrum shaping by filter Lyot is shown in **Figure 13(b)**. The optical spectrum showed a characteristic "bell" shape with a spectral FWHM bandwidth of 11 nm. Such a bandwidth provides smooth output pulse with width of intensity autocorrelation trace 305 fs that gives the pulse length of τ_{FWHM} = 182 fs for sech^2 pulse profile as shown in **Figure 13(d)**. This pulse length is close to the pulse length of 160 fs defined by aberrations in the stretcher-compressor module. To measure the ultrashort pulse width, we used a PulseCheck autocorrelator (APE GmbH). The inset of **Figure 13(d)** shows that there is no noticeable peak beyond the range of 1.5 ps.

Inserting a spectrum shaper inside the cavity of regenerative amplifier, we obtained approximately the same spectral width but less output power of about 20%. It is connected with accumulated effect of intra-cavity losses by Lyot filter inside the cavity. Thus combination of Lyot filter outside the cavity as a spectral shaper and identical pump power for two slabs in the dual-slab regenerative amplifier provides optimal condition of output power and pulse length.

Beam quality M^2 of output beam was below 1.2 at output power <12 W that allows the beam focusing to small spot size of 5–10 μm. High average output power, with more than tens of μJ, and beam quality are important for industrial microprocessing applications.

4. Microhole drilling for processing drawing dies using ultrafast Yb:KGW laser

Laser micromachining techniques are currently used due to the broad applications across the manufacturing sectors. Among the major applications, laser microhole drilling and cutting have much attention. For microhole drilling, the conventional fabrication method, lithography, which requires advanced facilities and numerous multiple steps, is limited in material type and geometry. Currently used drilling and cutting with nanosecond (ns) or longer pulsed laser are always accompanied with contamination to the surrounding material, melt zone, and

http://dx.doi.org/10.5772/64571

recast layer. Although the geometrical precision could be improved by using ns laser techniques, the quality and precision achievable are still limited due to the subsequently uncontrolled deposition of the melt. Due to the high energy input and thermally induced stress, drilling and cutting using picosecond pulsed laser still have disadvantages, e.g. cracks and heat-affected zone in the surrounding area. Not only the accuracy but also the reliability of the process is affected. For ultrafast lasers, energy deposition occurs on a timescale that is short compared to atomic relaxation processes. Ultrafast lasers suppress thermal diffusion and thus reduce heat-affected zone.

When processing transparent materials with ultrafast laser, the high intensity of focal volume induces multiphoton or tunnel ionization, and then subsequent electron heating or avalanche ionization, which gives rise to the efficient absorption of light. This phenomenon is observed by the nonlinear nature of the ultrafast laser interaction with the transparent materials. This generates the unique capability of transparent material processing using ultrafast laser.

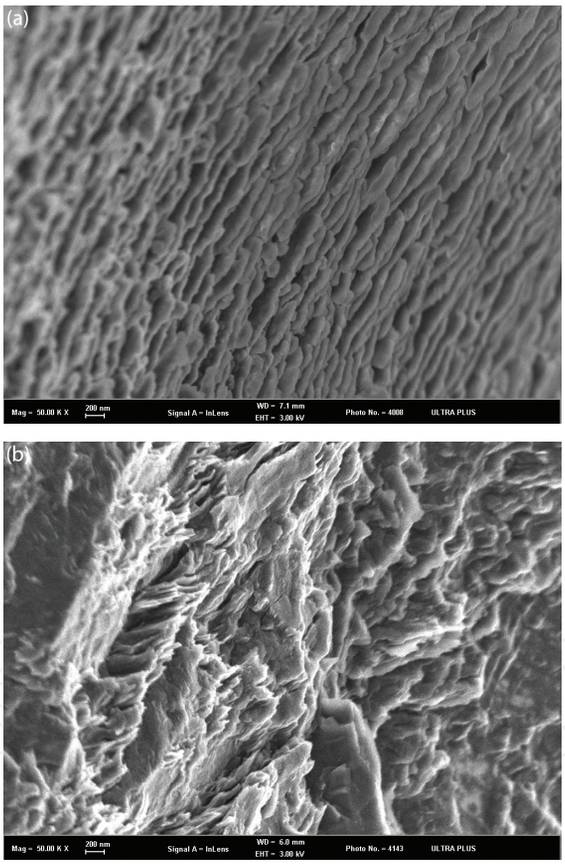

Figure 14. Scanning electron microscope (SEM) views of the structure on bearing land in drawing dies (a) using femtosecond (fs) laser and (b) using nanosecond (ns) laser.

Its promising application is drawing dies-hole drilling. Wire drawing is a deformation and metalworking process used to reduce the cross-section of a wire by pulling the wire through a drawing die. For drawing very fine wire, a single crystal diamond die is used. The drawing die consists of three zones: cone-shape entrance, bearing land, and back relief. The die bearing

determines the size of the wire. As demand for microwire increases across the manufacturing sectors, large scale machines are currently used to produce wire of microlevel, but it is not economical in an industry. Micromachining with ultrafast laser, which made the hole size small, has been reported. Smooth surfaces, also, are generally preferred for precision machining. **Figure 14** shows the SEM view of the bearing surface of drilled hole in dies. The comparison with fs and ns laser drilling results shows the advantage of fs laser drilling. **Figure 14(a)** shows a ripple for which spacing is generally <200 nm. The orientations of the ripple structures are parallel to each other. Similar ripple structure has been observed in various materials for fs laser drilling. Uneven and rough structures are shown in **Figure 14(b)**. It is clear that the material removal during the dies-hole drilling is accomplished by the formation of melt. Compared with two methods, micromachining with ultrafast laser creates much cleaner and smoother hole.

Ultrafast laser micromachining is an emerging technology for high-precision and cold-ablation material processing. For its advantages and potential uses, suitable ultrafast laser and laser operating parameters such as wavelength, repetition rate, average power, pulse duration, spot size, beam quality, and sample moving speed must be selected to achieve desired high-quality micromachining. In the near future, ultrafast laser micromachining will be used in various sectors including sub-micron material processing, surface structuring, photonics devices, biomedical devices, microfluidics, displays, and solar applications.

5. Conclusion

In conclusion, a room-temperature, diode-pumped, dual-crystal Yb:KGW laser operating as a Q-switched oscillator or regenerative amplifier has been developed where the gain bandwidth was extended by using N_g-cut + N_p-cut or N_g-cut + N_g-cut configuration. It was shown that fine-tuning the mode sizes in the crystals in the resonator with high pump power is important to obtain the maximal output power since thermal effects change the operation point in the stability zone and mode matching conditions. It was demonstrated simply by shifting the position of the end mirror along optical axis in the resonator. Optimization of the laser resonator increased the output power from 18 to 24 W in case of Q-switched oscillator and from 17 to 21 W in case of regenerative amplifier. Such optimization of laser resonator improves not only output power but also stability of laser operation, especially for N_g-cut + N_g-cut crystal configuration, that is manifest in reduction of output power fluctuations.

The use of this regenerative amplifier enabled to create compact, high average power, high brightness, diode-pumped femtosecond Yb:KGW laser system. This laser, which utilized a CPA MOPA laser scheme, consisted of master oscillator, regenerative amplifier, and stretcher-compressor module. It was capable of delivering 15 W of average output power with a pulse duration down to 182 fs high in a nearly diffraction limited output beam (M^2~1.2) at pulse repetition rates of 50–500 kHz.

This level of output power and quality of a laser beam are practically the same as the output power of Yb:KGW/Yb:KYW thin-disk lasers with medium level of output power [6, 9].

http://dx.doi.org/10.5772/64571

However laser heads based on volume laser media are considerably easier and cheaper compared with those based on thin-disk configuration. Subsequent development of multi-crystal laser approach will be able to increase output power on the level of high-power thin-disk lasers.

The achieved level of radiation parameters allows to successfully use this femtosecond laser for ultrafast micromachining in various applications including sub-micron material processing, surface structuring, creating photonics devices, biomedical devices, microfluidics, displays, and solar applications.

Acknowledgements

Parts of this chapter are reproduced from authors' previous publications [15, 25, 26].

Author details

Guang-Hoon Kim[1*], Juhee Yang[1], Byunghak Lee[1], Bosu Jeong[1], Sergey Chizhov[1], Elena Sall[1], Vladimir Yashin[2] and Uk Kang[1]

*Address all correspondence to: ghkim@keri.re.kr

1 Advanced Medical Device Research Division, Korea Electrotechnology Research Institute, Ansan-si, Republic of Korea

2 State Optical Institute, St. Petersburg, Russia

References

[1] Dausinger F., Lichtner F., and Lubatschowski H. (2004) Femtosecond Technology for Technical and Medical Applications. Berlin: Springer.

[2] Diels J.-C. and Rudolph W. (2006) Ultrashort Laser-Pulse Phenomena: Fundamentals, Techniques, and Applications on Femtosecond Time Scale. Boston: Academic Press.

[3] Fermann M. E., Galvanauskas A., and Sucha G. (2003) Ultrafast Lasers: Technology and Applications. New York: Marcel Dekker.

[4] Kuleshov N. V., Lagatsky A. A., Podlipensky A. V., Mikhailov V. P., and Huber G. (1997) Pulsed laser operation of Yb-doped $KY(WO_4)_2$ and $KGd(WO_4)_2$. Opt. Lett. 22: 1317–1320.

[5] Liu H., Nees J., Mourou G., Biswal S., Spuehler G.J., Keller U., and Kuleshov N. V. (2002) Yb:KGd(WO_4)$_2$ chirped-pulse regenerative amplifiers. Opt. Commun. 203: 315–321.

[6] Nickel D., Stolzenburg C., Giesen A., and Butze F. (2004) Ultrafast thin-disk Yb:KY(WO_4)$_2$ regenerative amplifier with a 200-kHz repetition rate. Opt. Lett. 29: 2764.

[7] Barty C., Korn G., Raksi F., Rose-Petruck C., Squier J., Tian A., Wilson K., Yakovlev V., and Yamakawa K. (1996) Regenerative pulse shaping and amplification of ultrabroadband optical pulses. Opt. Lett. 21: 219–221.

[8] Raybaut P., Balembois F., Druon F., and GeorgesP. (2005) Numerical and experimental study of gain narrowing in ytterbium-based regenerative amplifiers. IEEE J. Quantum Electron. 41: 415–426.

[9] Buenting U., Sayinc H., Wandt D., Morgner U., and Kracht D. (2009) Regenerative thin disk amplifier with combined gain spectra producing 500 mJ sub 200 fs pulses. Opt. Express 17: 8046–8050.

[10] Strickland D., and Mourou G. (1985) Compression of amplified chirped optical pulses. Opt. Commun. 56: 219–221.

[11] Kim G. H., Kang U., Heo D., Yashin V. E., Kulik A. V., Sall' E. G., and Chizhov S. A. (2010) A compact femtosecond generator based on an Yb:KYW crystal with direct laser-diode pumping. J. Opt. Technol. 77: 225–229.

[12] Software package for LASer Cavity Analysis and Design (LAS-CAD). 1996–2015 LAS-CAD GmbH, Germany, www.las-cad.com.

[13] Brunner F., et al. (2000) Diode-pumped femtosecond Yb:KGd(WO_4)$_2$ laser with 1.1-W average power Opt. Lett. 25: 1119.

[14] Buettner A., Buenting U., Wandt D., Neumann J., and Kracht D. (2010) Ultrafast double-slab regenerative amplifier with combined gain spectra and intracavity dispersion compensation. Opt. Express 18(21): 21973–21980.

[15] Kim G. H. Yang J., Chizhov S. A., Sall E. G., Kulik A. V., Yashin V. E., Lee D. S., and Kang U. (2012) High average-power ultrafast CPA Yb:KYW laser system with dual-slab amplifier Opt. Express 20: 3434–3442.

[16] Koechner W. (2006) Solid-state Laser Engineering. New York: Springer.

[17] International Standard ISO 11670:2003: Lasers and Laser-related Equipment – Test Methods for Laser Beam Parameters – Beam Positional Stability. This standard was last reviewed in 2015.

[18] Kim G. H., Yang J., Lee B., Sall E. G., Chizhov S. A., Yashin V. E., and Kang U. (2015) Investigation of diode-pump absorption efficiency and thermo-optical effects in a high-power Yb:KGW laser. Quantum Electron. 45: 211–215.

[19] Biswal S., O'Connor S. P., Bowman S. R. (2005) Thermo-optical parameters measured in ytterbium-doped potassium gadolinium tungstate. Appl. Opt. 44: 3093–3097.

[20] Chenais S., Balembois F., Druon F., Lucas-Leclin G., and Georges P. (2004) Thermal lensing in diode-pumped ytterbium lasers – part I: theoretical analysis and wavefront measurements. IEEE J. Quantum Electron. 40: 1217–1234.

[21] Kim G. H., Yang J., Chizhov S. A., Sall E. G., Kulik A. V., Yashin V. E., Kang U. (2013) High brightness Q-switched oscillator and regenerative amplifier on dual-crystal Yb:KGW laser. Laser Phys. Lett. 10: 125004.

[22] Kim G. H., Yang J., Chizhov S. A., Sall E. G., Kulik A. V., Yashin V. E., Kang U. (2014) High-power directly diode-pumped femtosecond Yb:KGW lasers with with optimized parameters. Proc. of SPIE, 8959: 8959B-1–89591B-8.

[23] Kim G. H., Yang J. H., Lee D. S., Yashin V. E., Kulik A. V., Sall E. G., Chizhov S. A., Kang U. (2012) High power and high efficiency lasers on crystals Yb:KYW with end pumping operating in CW and pulsed regimes. Quantum Electron. 42: 292–297.

[24] Kim G. H., Yang J. H., Yashin V. E., Kulik A. V., Sall E. G., Chizhov S. A., Kang U. (2013) Power limitation and pulse distortions in Yb:KGW laser system with chirped pulse amplification. Quantum Electron. 43: 725–730.

[25] Kim G. H., Yang J., LeeD. S., KulikA. V., Sall'E. G., ChizhovS. A., YashinV. E., and KangU. (2012) Directly diode-pumped femtosecond laser based on an Yb:KYW crystal. Proc. SPIE 8247: 82471C.

[26] Kim G. H., Yang J., Sall E., Chizhov S., Kulik A., Lee D. S., Kang U., Yashin V. (2012) Development of compact femtosecond Yb: KYW oscillators: simulation and experiment. J. Korean Phys. Soc. 61: 365–370.

IntechOpen